Chaos
An Interdisciplinary Journal of Nonlinear Science

Noise-induced switching in an oscillator with pulse delayed feedback: A discrete stochastic modeling approach

Cite as: Chaos **32**, 093141 (2022); https://doi.org/10.1063/5.0100698
Submitted: 26 May 2022 • Accepted: 22 August 2022 • Published Online: 26 September 2022

Vladimir V. Klinshov and Otti D'Huys

COLLECTIONS

Paper published as part of the special topic on Non-smooth Dynamics

View Online Export Citation CrossMark

ARTICLES YOU MAY BE INTERESTED IN

Cluster synchronization induced by manifold deformation
Chaos: An Interdisciplinary Journal of Nonlinear Science **32**, 093139 (2022); https://doi.org/10.1063/5.0107866

Abrupt transition of the efficient vaccination strategy in a population with heterogeneous fatality rates
Chaos: An Interdisciplinary Journal of Nonlinear Science **32**, 093140 (2022); https://doi.org/10.1063/5.0087627

Learning spatiotemporal chaos using next-generation reservoir computing
Chaos: An Interdisciplinary Journal of Nonlinear Science **32**, 093137 (2022); https://doi.org/10.1063/5.0098707

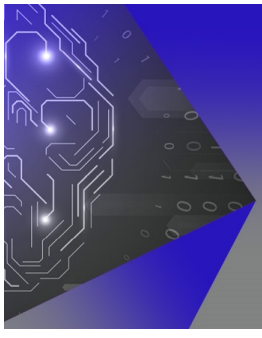

APL Machine Learning
Machine Learning for Applied Physics
Applied Physics for Machine Learning
Now Open for Submissions

AIP Publishing

© 2022 Author(s).

Noise-induced switching in an oscillator with pulse delayed feedback: A discrete stochastic modeling approach

Cite as: Chaos **32**, 093141 (2022); doi: 10.1063/5.0100698
Submitted: 26 May 2022 · Accepted: 22 August 2022 ·
Published Online: 26 September 2022

View Online Export Citation CrossMark

Vladimir V. Klinshov[1,2,a] and Otti D'Huys[3,b]

AFFILIATIONS

[1]Institute of Applied Physics of the Russian Academy of Sciences, 46 Ul'yanov Street, Nizhny Novgorod 603950, Russia
[2]Higher School of Economics, National Research University, 25/12 Bol'shaya Pecherskaya Street, Nizhny Novgorod 603155, Russia
[3]Department of Applied Computing Sciences, Maastricht University, P.O. Box 616, 6200 MD Maastricht, The Netherlands

Note: This article is part of the Focus Issue, Non-smooth Dynamics.
[a]**Author to whom correspondence should be addressed:** vladimir.klinshov@ipfran.ru
[b]**Electronic mail:** o.dhuys@maastrichtuniversity.nl

ABSTRACT

We study the dynamics of an oscillatory system with pulse delayed feedback and noise of two types: (i) phase noise acting on the oscillator and (ii) stochastic fluctuations of the feedback delay. Using an event-based approach, we reduce the system dynamics to a stochastic discrete map. For weak noise, we find that the oscillator fluctuates around a deterministic state, and we derive an autoregressive model describing the system dynamics. For stronger noise, the oscillator demonstrates noise-induced switching between various deterministic states; our theory provides a good estimate of the switching statistics in the linear limit. We show that the robustness of the system toward this switching is strikingly different depending on the type of noise. We compare the analytical results for linear coupling to numerical simulations of nonlinear coupling and find that the linear model also provides a qualitative explanation for the differences in robustness to both types of noise. Moreover, phase noise drives the system toward higher frequencies, while stochastic delays do not, and we relate this effect to our theoretical results.

Published under an exclusive license by AIP Publishing. https://doi.org/10.1063/5.0100698

Pulse-like interactions appear in neuronal populations, optical setups, electronic oscillators, and various other systems. Such interactions typically lead to non-smooth dynamics: the reception of a pulse leads to an abrupt change of the system state, which becomes an instant "jump" in the limit of infinitely short pulses. Here, we consider the non-smooth dynamics of an oscillator with pulse self-coupling. The feedback loop contains a temporal delay, and the system is also subject to noise. We consider two types of stochastic perturbations: noise acting on the oscillator, and perturbations acting on the delay line. We show that these different sources of noise both induce switching between different coexisting states, but the system shows opposite scaling properties of the switching characteristics. We use an event-based approach to derive a stochastic map describing the system evolution from one pulse to the next. For weak noise, after linearization, the map has the form of an autoregressive process, which allows us to obtain detailed statistics of the system fluctuations. As the noise level increases, we observe switching events between different metastable states of the system. We obtain analytical expressions for the switching characteristics, which provide an accurate description of the linearized system and offer a qualitative explanation for the switching dynamics for general coupling functions.

I. INTRODUCTION

Systems with pulse-like interactions, i.e., signals with a short duration compared to other characteristic time scales, are ubiquitous in nature. Such systems include populations of biological neurons,[1] cardiac cells,[2] wireless networks,[3] chemical and electronic oscillators,[4–7] optical systems,[8] and many others. In the limit of infinitely short pulses, the dynamics of such systems becomes non-smooth since the system state changes instantly at the moment of pulse arrival. A common approach to studying non-smooth dynamics of oscillatory systems with pulse interaction is to describe the

Published under an exclusive license by AIP Publishing

oscillator by its phase and the interaction by the so-called phase resetting curve (PRC).[9] The PRC describes how the input pulse delays or advances the oscillator depending on the momentary phase of the oscillator when the pulse is received. Models of pulse-coupled phase oscillators interacting via phase resetting curves have been shown to display a variety of dynamical behavior, such as synchronous[10,11] and asynchronous[12,13] states, as well as clustered[14,15] and splay states.[16]

Due to the non-smooth nature of pulse-coupled systems, discrete maps are a natural tool to explore their dynamics. Such maps describe the system evolution from one pulse to another and allow one to study its dynamics numerically or analytically. Moreover, the map-based approach remains applicable even if the propagation of pulses in the system takes a finite time.[17,18] Thus, pulse-coupled systems provide a convenient framework to study the effect of temporal delays, since the pulse nature of the interactions ensures finite-dimensional dynamics. The underlying reason is that only the (discrete) moments of pulse emission play a role in the future dynamics, not the (continuous) history of the system in a delay window.

The role of delay on the non-smooth dynamics of pulse-coupled oscillators has been extensively studied, in small motifs of only a few elements[19–22] and in large ensembles.[23,24] Delays were shown to cause multistability in recurrent neural loops[25,26] and lead to the emergence of complex high-period and chaotic behavior in oscillatory systems with pulse feedback.[27,28]

In this paper, we extend our earlier work[29] and show that pulse-interacting systems are well suited to study the effect of stochastic fluctuations of different types, thanks to the discrete nature of the coupling. In particular, we consider an oscillator with pulse delayed coupling and introduce noise of two types: (i) phase noise acting on the oscillator and (ii) stochastic fluctuations of the coupling delay. The model of the oscillator with pulse delayed feedback is formulated and described in Sec. II.

In Sec. III, we introduce noise to the model. In contrast to Ref. 29, this model contains both types of noise simultaneously. We show that the map-based approach still can be applied to describe the noisy dynamics of the system and propose the event-based integration scheme that we use for numerical simulations of the system. We approximate the dynamics of the system in the limit of weak noise in Sec. IV: we show that if the system fluctuates around a deterministic state, the dynamics is well described by an autoregressive process. For stronger noise, the map-based approach sheds light on the system switching between different deterministic states. Our theory allows us to predict the lifetimes of different states and their scaling, in the case of a linear PRC. The most prominent finding is a significant dependence of the scaling of the lifetimes on the noise type: For stochastic delays, the lifetimes decrease exponentially with the coupling strength, but for phase noise, the dependence is non-monotonous with a pronounced maximum. A similar effect was described numerically already in Ref. 29; however, in the case of phase noise, the theoretical explanation relied on a comparison with the continuously coupled system, which is only valid for weak coupling. In particular, this did not allow us to discover the decrease of the lifetimes for strong coupling in the case of phase noise. The map-based approach in this paper is valid for stronger coupling as well, so we replenish the omission of the earlier work and provide a solid theoretical ground for the problem.

In Sec. V, we show numerically the scaling properties for nonlinear coupling functions. Although the linear model does not provide a quantitatively accurate estimate of lifetime in this case, the qualitative behavior is well captured by the linear model. Moreover, we discover a novel effect of speeding up the dynamics by phase noise compared to stochastic delays, and we provide an explanation for this effect with our linear theory. Finally, we briefly summarize our results in Sec. VI.

II. MODEL

We start by introducing the deterministic model for a phase oscillator subject to pulse delayed feedback,[27]

$$\frac{d\theta(t)}{dt} = 1 + \epsilon Z(\theta(t-0)) \sum_{t_s} \delta(t - t_s - \tau). \tag{1}$$

The oscillator's phase $\theta(t)$ evolves with a natural frequency that we normalized to 1; each time when it reaches unity, the oscillator emits a pulse and the phase is reset to 0. These moments of pulse emission are denoted as t_s. The emitted pulses are sent into a delay line and arrive back at the oscillator after a delay time τ. The arrival of a pulse causes an instant phase shift, the magnitude of this shift is determined by the phase resetting curve $Z(\theta)$ and the feedback strength ϵ,

$$\theta(t+0) = \theta(t-0) + \epsilon Z(\theta(t-0)), \tag{2}$$

where $\theta(t-0)$ and $\theta(t+0)$ denote the phase before and after the reception of the pulse, respectively.

System (1) was studied in detail in Ref. 28, we briefly discuss the main dynamical regimes in the following. We look at the phase evolution between the emission of a pulse, at $t = t_{s_0}$, and reception of the same pulse, at $t = t_{s_0} + \tau \equiv t^*$. This pulse arrives during a later inter-spike interval, so we have $t_{s-1} < t^* < t_s$, for some integer $s > s_0$. We can write for the total phase increment $\Delta\theta_s$ between t_{s_0} and t^*,

$$\Delta\theta_s = \tau + \epsilon \sum_{t_{s_0} < t_k + \tau < t^*} Z(\theta(t_k + \tau)), \tag{3}$$

where the first term corresponds to the increment due to the constant speed and the second term represents the phase shifts due to the pulses arriving during the past delay interval. Note that in this expression, we did not take into account the phase resets from one to zero each time when the oscillator emits pulses. Thus, in order to obtain the reception phase $\psi_s = \theta(t^* - 0)$, one needs to subtract the number of completed cycles C_s within the past delay interval. Since $\theta(t_{s_0}) = 0$, one obtains

$$\psi_s = \Delta\theta_s \bmod 1 = \Delta\theta_s - C_s. \tag{4}$$

Note that C_s equals the number of pulse timings stored in the delay line (without counting the pulse at $t = t^*$) and $C_s + 1 = s - s_0$; therefore, we call it the "capacity" of the system. The deterministic dynamics of system (1) and the main variables used in the model are sketched in Fig. 1. From Eqs. (3) and (4), one can define the (mean)

Published under an exclusive license by AIP Publishing

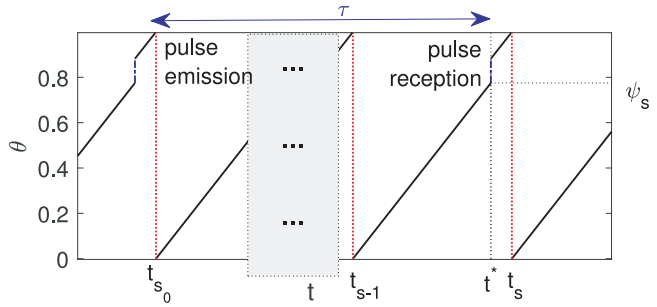

FIG. 1. Sketch of the typical deterministic dynamics of a pulse-coupled oscillator with delayed feedback. The phase shift due to pulse reception is indicated in blue, and the pulse emission and subsequent phase resetting events in red. The timings and phases used in the model description are also indicated.

frequency ω_s as the phase increment per delay interval,

$$\omega_s = \frac{\Delta\theta_s}{\tau} = \frac{C_s}{\tau} + \frac{\psi_s}{\tau} = 1 + \frac{\epsilon}{\tau}\sum_{k=s-C_s}^{s-1} Z(\psi_k). \tag{5}$$

The dynamics of spiking oscillators is most often characterized by the inter-spike intervals (ISIs) $T_s = t_s - t_{s-1}$. The frequency ω_s relates to the average inter-spike interval over the past delay window in the following way: since we have that $\sum_{k=s-C_s}^{s-1} T_k = C_s - \epsilon\sum_{k=s-C_s}^{s-1} Z(\psi_k)$, we find

$$\omega_s = 1 + \frac{C_s}{\tau}\left(1 - \langle T_s\rangle\right), \tag{6}$$

where $\langle T_s\rangle = \frac{1}{C_s}\sum_{k=s-C_s}^{s-1} T_k$ (here and further, by $\langle\cdot\rangle$, we denote averaging over all the complete ISIs in the delay line). This relation depends on the temporal capacity C_s, but this dependence is not strong. As long as the coupling is relatively weak (which is an assumption for the validity of phase models) and the delay is large enough, we have $C_s/\tau \approx 1$, and $\omega_s \approx 2 - \langle T_s\rangle$.

We mostly record the frequency ω_s and not the interspike interval T_s for several reasons. First, the frequency ω_s allows direct comparison to continuously coupled phase oscillators.[30] Also there, a description of the stochastic system is based on the average frequency per delay interval. Second, a single instance $\omega_s = (\psi_s + C_s)/\tau$ is related to the interspike interval $\langle T_s\rangle$ averaged over C_s instances; thus, the frequency shows less fluctuations than the ISIs and allows direct numerical processing. This is illustrated in Sec. III [see Figs. 4(a)–4(c)].

To find the main deterministic regimes, we combine Eqs. (3) and (4) and obtain a nonlinear map in the reception phases ψ_s, with dimension C_s,

$$\psi_s = (\tau - C_s) + \epsilon\sum_{k=s-C_s}^{s-1} Z(\psi_k). \tag{7}$$

It was shown that under quite general assumptions on the phase response function $Z(\cdot)$, the deterministic system dynamics unfolds in such a way that exactly one pulse arrives to the oscillator between any two consecutive moments of the pulse emission.[28] In that case, the capacity of the dynamical regime stays constant $C_s \equiv C$, and the map provides a valid description of such a regime with a specific capacity C. Note, however, that the capacity is not a characteristic of the system itself but a characteristic of the regime it is in. Further, we show that the system might be multistable, i.e., has several regimes with different capacities for the fixed set of parameters.

The fixed points of the map Eq. (7) correspond to the basic periodic regimes and are characterized by a constant capacity C and a constant reception phase ψ_C. They can be found by solving

$$\psi_C = \tau - C + \epsilon C Z(\psi_C). \tag{8}$$

Consequently, the frequency ω_C and the inter-spike interval T_C are also constant, they are given, respectively, by $\omega_C = \frac{\psi_C + C}{\tau}$ and $T_C = 1 - \epsilon Z(\psi_C)$.

Clearly, the number of solutions with different capacities increases with the coupling strength ϵ and the feedback delay τ. Solutions for which $-1 < \epsilon Z'(\psi) < \frac{1}{C}$ holds are stable.[28] For a PRC that fulfills $Z(0) = Z(1) = 0$, meaning that the phase does not change when a pulse is received at the moment of spiking, this results in a stable "basic solution," with a capacity $C^* = \lfloor\tau\rfloor$, the largest integer not greater than τ. This capacity corresponds to the number of natural cycles within a delay interval. For vanishing coupling strength $\epsilon \to 0$, we have $T_{C^*} \to 1, \omega_{C^*} \to 1$, and $\psi_{C^*} \to \tau - C^*$. As the coupling strength ϵ increases, solutions with a different capacity C emerge in saddle-node bifurcations, in the following, we denote the frequency, inter-spike interval, and reception phase associated with the stable solution as ω_C, T_C, and ψ_C, respectively.

We show this structure for two different phase response curves in Fig. 2. First, we consider the PRC $Z(\theta) = \frac{1}{2\pi}\sin(2\pi\theta)$. This is the pulse-coupled version of a regular Hopf normal form oscillator[31] and can both delay and speed up the oscillator, depending on the reception phase. It allows direct comparison with sinusoidally coupled phase oscillators with continuous coupling. The frequencies and interspike intervals of the different regular spiking regimes are shown in Figs. 2(a) and 2(b) for increasing coupling strength. In order to illustrate the emergence of multiple solutions, we select a relatively large value of the delay $\tau = 15.95$, for which we have the basic solution with capacity $C^* = 15$ always stable. As ϵ increases, solutions with $C = 16$, $C = 14$, and $C = 17$ emerge; solutions with the highest capacity correspond to the highest frequency, and the smallest ISI. The set of solutions is approximately centered around the natural frequency $\omega = 1$ (both in terms of the frequencies and in terms of the ISIs), the structure of the solution set is reminiscent of the frequency locked states in coupled phase oscillators with continuous sinusoidal coupling.[30] This set of solutions also reminds us of the external cavity modes in semiconductor lasers with delayed feedback,[33] a similarity that results from the sinusoidal coupling term.

Second, we consider a PRC $Z(\theta) = \frac{1}{2\pi}(1 - \cos(2\pi\theta))$; this PRC resembles a θ-neuron.[32] This cosine PRC is always positive, and, thus, the phase is always advanced due to an incoming pulse. In Figs. 2(c) and 2(d), we show the frequencies and ISIs of the basic regimes for the same value of the delay $\tau = 15.95$; the basic solution with $C^* = 15$ is also present here. In contrast to the sinusoidal coupling, only solutions with higher frequency and smaller ISI emerge

Published under an exclusive license by AIP Publishing

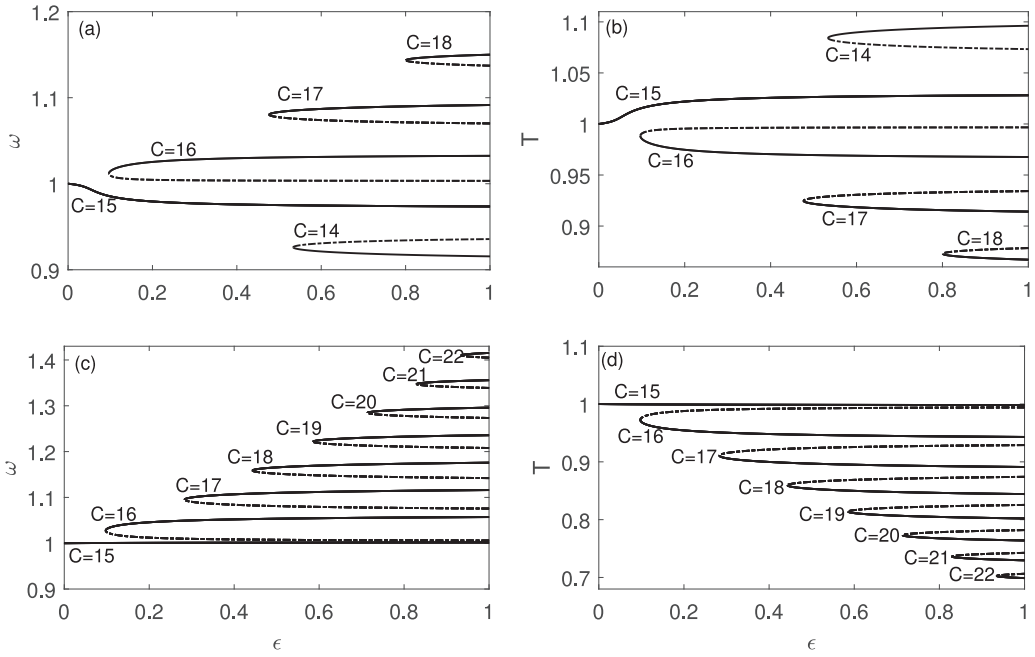

FIG. 2. Frequencies [(a) and (c)] and inter-spike interval [(b) and (d)] of the regular spiking solutions, for varying coupling strength ϵ. Full lines correspond to stable solutions, and dashed lines represent unstable solutions. $Z(\theta) = \frac{1}{2\pi}\sin(2\pi\theta)$ [(a) and (b)] and $Z(\theta) = \frac{1}{2\pi}(1-\cos(2\pi\theta))$ [(c) and (d)] and $\tau = 15.95$.

as ϵ increases: for our choice of parameters, solutions with capacities $C = 16$ to $C = 22$ consecutively appear.

III. STOCHASTIC MODEL AND INTEGRATION SCHEME

We described in Sec. II, the deterministic system [Eq. (1)] with multiple stable coexisting states, we now consider the effect of stochastic fluctuations. Since the system consists of two major components, the oscillator and the delay line, we introduce two different types of stochastic perturbations: those acting on the oscillator and those acting on the feedback delay. The system with these two types of noise is governed by the equation

$$\frac{d\theta}{dt} = 1 + \epsilon Z(\theta(t-0)) \sum_{t_s} \delta(t - t_s - (\tau + \gamma\xi_s)) + \sigma\eta(t). \quad (9)$$

The stochastic perturbations on the oscillator are modeled by an additive noise term $\sigma\eta(t)$, with $\eta(t)$ a standard Gaussian white noise with $\langle\eta(t)\eta(t')\rangle = \delta(t-t')$ and σ^2 the noise intensity. We call this additive noise acting on the oscillator "phase noise." The stochastically varying delay is implemented in the following way: the delay of the pulse being received in the sth ISI is given by $\tau + \gamma\xi_s$, with ξ_s a random deviation, and γ^2 is the intensity of the delay fluctuations. The deviations ξ_s are assumed to be independent and normally distributed with zero mean and unit variance. We always chose γ small and truncate the distribution, so that the delay remains positive and the pulse order does not change. Note that the system with pulse coupling is quite convenient for the introduction of randomly varying delays because of the discrete nature of the pulses.

Since the pulse nature of the system preserves in the presence of noise, its dynamics again unfolds as a sequence of discrete events corresponding to the emission and the reception of the pulses. We trace the system dynamics starting from $t_0 = 0$ and an arbitrary initial phase $\theta_0 \in (0, 1)$. While the oscillator does not receive or emit pulses, the phase evolution is Brownian motion with drift,

$$\frac{d\theta}{dt} = 1 + \sigma\eta(t). \quad (10)$$

This process is interrupted by a discrete event of one of the two types. The first possible event is that the phase reaches unity at $t = t_s$, and the oscillator emits a pulse. The probability distribution of this moment t_s, is an inverse Gaussian distribution with a mean $1 - \theta_0$,

$$f(t_s|\theta_0) = \frac{1-\theta_0}{\sigma\sqrt{2\pi(t_s-t_0)^3}} \exp\left(-\frac{(1-\theta_0-t_s)^2}{2\sigma^2 t_s}\right). \quad (11)$$

The second possibility is that the oscillator receives a pulse at $t = t^* < t_s$, i.e., before it reaches unity, t^* is the first timing stored in the delay line. In this case,[34] the distribution of the reception phase $\theta(t^*-0) \equiv \psi_s$ is given by

$$f(\psi_s|\theta_0, t^*) = \frac{1}{\sigma\sqrt{2\pi t^*}} \left\{ \exp\left[-\frac{(\psi_s-\theta_0-t^*)^2}{2\sigma^2 t^*}\right] - \exp\left[\frac{2-2\theta_0}{\sigma^2} - \frac{(2-\psi_s+\theta_0+t^*)^2}{2\sigma^2 t^*}\right]\right\}, \quad (12)$$

Published under an exclusive license by AIP Publishing

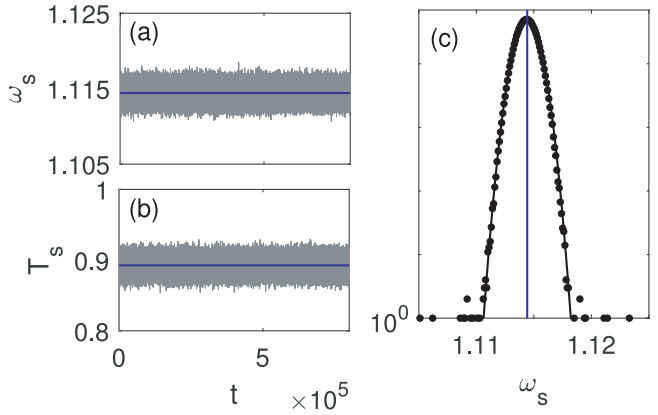

FIG. 3. Time trace of the frequency (a), ISIs (b), and frequency histogram (blue dots) (c) (in logarithmic scale). We compare the frequency distribution to the theoretical weak noise approximation (full black line) [Eq. (29)], and the deterministic solution with $C = 17$ is indicated by the full blue line. Parameters are $\epsilon = 0.8$, $\tau = 15.95$, $\sigma = 0.01$ and $\gamma = 0$, and $Z(\theta) = \frac{1}{2\pi}(1 - \cos(2\pi\theta))$.

where we used an absorbing boundary condition $f(1|\theta_0, t^*) = 0$. Note that the integral $\int_{-\infty}^{1} f(\psi_s|\theta_0, t^*)d\psi_s = P_1 < 1$, which corresponds to a non-zero flow through the boundary.

This notion of the two types of possible discrete events leads to a simple event-based integration scheme: at any time t and oscillator phase $\theta(t)$, we generate the next spike timing t_s according to the distribution (11) and compare to the first pulse reception time t^* that is stored in the delay line. Then two different outcomes are possible: (i) With a probability P_1, we have $t_s > t^*$. In this case, the next event is the arrival of a pulse. We generate the reception phase $\theta(t^* - 0) = \psi_s$ according to the distribution (12), then we update the phase to $\theta(t^* + 0) = \psi_s + \epsilon Z(\psi_s)$ and update time to $t = t^*$. The pulse at $t = t^*$ is removed from the delay line. (ii) With a probability $P_2 = 1 - P_1$, we have $t_s < t^*$, and the oscillator emits a pulse before it receives one. We then update time to $t = t_s$ and reset the oscillator phase. We add a new spike reception time $t^* = t_s + \tau + \gamma\xi_{s+C_s}$ to the delay line.

After each of these outcomes, we repeat the same procedure, which allows us to simulate the system dynamics for an arbitrarily long time. Figures 3 and 4 show two examples of the simulation with the cosine PRC, for weak and strong noise, respectively. The initial phase was selected randomly in both cases, while in the delay line, pulses were stored at integer values of time (corresponding to the natural cycle). For weak noise (illustrated in Fig. 3), we see that the frequency ω_s, plotted in panel (a), and the inter-spike intervals T_s, plotted in panel (b), fluctuate near the values corresponding to the regular spiking solution of the deterministic system with $C = 17$, indicated by the full blue line. Note that the magnitude of the fluctuations is much larger for the inter-spike intervals T_s than for the frequency ω_s, since the frequency depends on the averaged inter-spike interval. We also show the distribution of the frequency in panel (c).

For strong noise, shown in Fig. 4, we see in the time trace of the frequency [Fig. 4(a)], apart from the fluctuations near the deterministic solutions, sporadic hopping from one solution to another. In particular, the system switches between the two solutions with $C = 17$ and $C = 18$. Note that the boundary between the two regimes corresponds to $\omega\tau = C + \psi_u$, with ψ_u the reception phase associated with the unstable state between two stable regimes. These hopping events are also visible in the time trace of the averaged ISI [Fig. 4(c)].

Note that, for the cosine PRC, the temporal capacity C_s switches constantly, without this indicating a hopping event. This is because, for the central frequencies, we have $\psi_C \approx \frac{3}{4}$, while $\psi_u \approx \frac{1}{4}$. This means that pulse reception and pulse emission do not necessarily alternate; pulse reception is typically at three quarters of a cycle, but may vary between a quarter in the same cycle, and a quarter into the next cycle.

In contrast, for the sinusoidal PRC, as the delay time and coupling strength increase, we have that, for a solution with fixed capacity $\psi_u \to 0$ (for $C < C^*$) or $\psi_u \to 1$ (for $C > C^*$) as the coupling strength ϵ increases. Hence, for large enough delays, the temporal capacity C_s does indicate effectively the regime of the oscillator. Thus, if the oscillator does not receive a pulse within an ISI, or receives two pulses within an ISI, this typically indicates a hopping event to another regime.

IV. WEAK NOISE APPROXIMATION

A. Derivation of an autoregressive process

The integration scheme is exact, but the probability distributions (11) and (12) do not allow for straightforward insight into the system behavior. In the following, we study the dynamics in the limit of weak noise $\sigma \ll 1$ and $\gamma \ll 1$, when the probability distributions (11) and (12) can be approximated by normal distributions. For weak noise, the system fluctuates around a deterministic solution with a fixed capacity C, as illustrated by the numerical simulations shown in Fig. 3. We can also assume pulse reception and emission alternate. Under these assumptions, we show that it is possible to approximate the dynamics as an autoregressive process.

We model the system in terms of the deviations x_s in the spike reception timings within an interspike interval,

$$x_s = t^* - t_{s-1} - \psi_C, \tag{13}$$

and the deviations y_s of the interspike intervals,

$$y_s = T_s - T_C = t_s - t_{s-1} - T_C. \tag{14}$$

We follow the dynamics between two pulse emissions. At $t = t_{s-1}$, the phase is reset, $\theta(t_{s-1}) = 0$. Since we assume that the emission and reception of a pulse alternate, the next event is the reception of a pulse, at $t = t^* = t_{s-1} + \psi_C + x_s$. During the time between these events, the phase experiences Brownian motion [Eq. (10)]. Thus, before the pulse reception, the reception phase $\theta(t^* - 0) = \psi_s$ is distributed according to (11), which we approximate by a normal distribution with mean $\psi_C + x_s$, and variance $\sigma^2(\psi_C + x_s) \approx \sigma^2\psi_C$. Here, we use that the noise strength σ^2, and the deviations x_s from the deterministic state are small, and we only

Published under an exclusive license by AIP Publishing

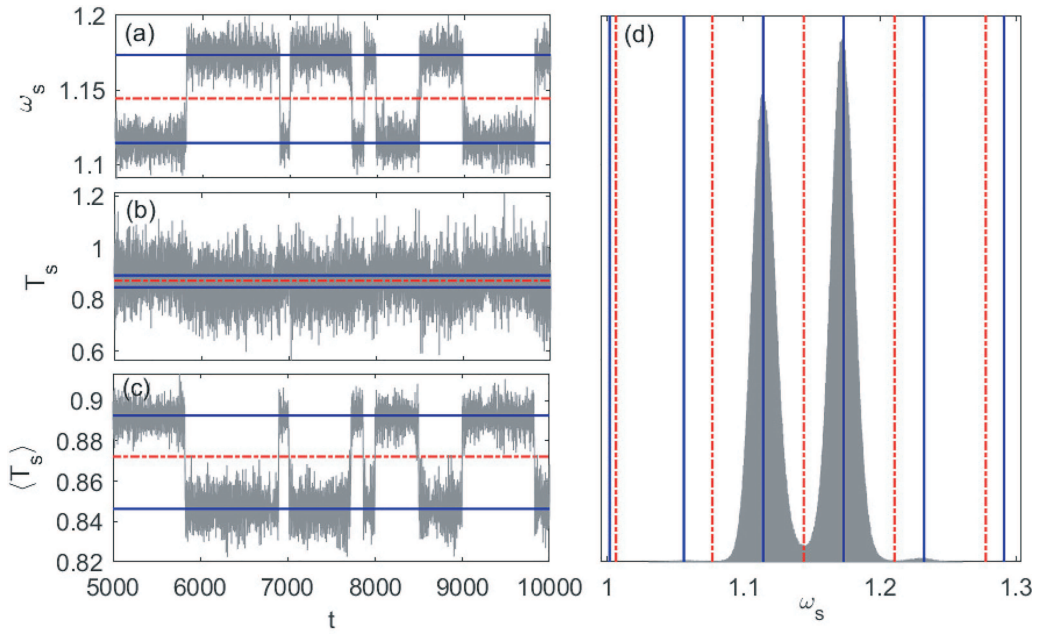

FIG. 4. (a) Time trace of the frequency, (b) ISIs, (c) ISI averaged over a window of 17 occurrences, and (d) frequency histogram. We added the deterministic solutions: solid blue lines denote the stable regimes, and dotted-dashed red lines correspond to unstable regimes. In panel (d), all deterministic solutions are shown; in panels (a)–(c), only those that play a role in the dynamics. Parameters are $\epsilon = 0.8$, $\tau = 15.95$, $\sigma = 0.1$ and $\gamma = 0$, and $Z(\theta) = \frac{1}{2\pi}(1 - \cos(2\pi\theta))$.

consider first order terms. This leads to

$$\psi_s = (t^* - t_{s-1}) + \sqrt{t^* - t_{s-1}}\eta_1 \approx \psi_C + x_s + \sigma\sqrt{\psi_C}\eta_1, \quad (15)$$

where η_1 is a standard Gaussian random number. After receiving the pulse, the phase becomes

$$\begin{aligned}\theta(t^* + 0) &= \psi_s + \epsilon Z(\psi_s) \\ &\approx (\psi_C + \epsilon Z(\psi_C)) + (1 + \epsilon Z'(\psi_C))(x_s + \sigma\sqrt{\psi_C}\eta_1),\end{aligned} \quad (16)$$

where we use a linear approximation of the PRC, as the deviations from the deterministic state are small.

The next event is pulse emission, at $t = t_s$. The time until the phase reaches unity, and emits the next pulse, is given by Eq. (11). For weak noise, we approximate the inverse Gaussian distribution by a Gaussian distribution with mean $1 - \theta(t^* + 0)$ and variance $\sigma^2(1 - \theta(t^* + 0)) \approx \sigma^2(T_C - \psi_C)$. We find

$$\begin{aligned}t_s &= t^* + (1 - \theta(t^* + 0)) + \sigma\sqrt{1 - \theta(t^* + 0)}\eta_2 \\ &\approx t_{s-1} + T_C - \epsilon Z'(\psi_C)x_s \\ &\quad - \sigma\left(\sqrt{\psi_C}(1 + \epsilon Z'(\psi_C))\eta_1 - \sqrt{T_C - \psi_C}\eta_2\right),\end{aligned} \quad (17)$$

where η_2 is another independent standard Gaussian random number. Finally, we find for the deviation of the inter-spike interval $y_s = T_s - T_C = t_{s+1} - t_s - T_C$,

$$y_s = -\epsilon Z'(\psi_C)x_s + \sigma\sqrt{\psi_C(1 + \epsilon Z'(\psi_C))^2 + (T_C - \psi_C)}\eta_s. \quad (18)$$

Here, we combined the two random Gaussian terms proportional to η_1 and η_2 to a single term proportional to the standard Gaussian random number η_s.

In order to find a second equation relating the deviations x_s and y_s, we use the relation between emission time t_{s-C-1} and reception time t^* of the same pulse,

$$t^* = \tau + \gamma\xi_s + t_{s-C-1}.$$

We can write, using Eq. (13),

$$\begin{aligned}t^* - t_{s-1} = \psi_C + x_s &= (\tau + \gamma\xi_s) - (t_{s-1} - t_{s-C-1}) \\ &= (\tau + \gamma\xi_s) - \sum_{k=s-C}^{s-1} T_k.\end{aligned} \quad (19)$$

Subtracting the deterministic values, we find

$$x_s = \gamma\xi_s - \sum_{k=s-C}^{s-1} y_k. \quad (20)$$

Finally, we obtain a single equation for y_s by combining Eqs. (18) and (20),

$$y_s = \epsilon Z'(\psi_C) \sum_{k=s-C}^{s-1} y_k + \nu_z z_s, \quad (21)$$

where z_s is a standard Gaussian random number and ν_z is given by

$$\nu_z = \left(\epsilon Z'(\psi_C)\right)^2 \gamma^2 + \left(\psi_C(1 + \epsilon Z'(\psi_C))^2 + (T_C - \psi_C)\right)\sigma^2. \quad (22)$$

Published under an exclusive license by AIP Publishing

B. Analysis of the autoregressive process

The process equation (21) constitutes an autoregressive process of order C (AR(C)); the solution is stationary if the corresponding deterministic solution is stable. It is straightforward to compute the autocorrelation function.[38] By taking the time-average of both sides of Eq. (21), we quickly find that $\langle y_s \rangle = 0$, i.e., the distribution of ISIs is indeed centered around the deterministic value T_C. Next, we multiply the equation with y_{s-n}, $1 \le n \le C$, average over time and normalize by the variance $v_y = E(y_s^2)$ [where $E(\cdot)$ denotes the mean over the time trace]. This leads to the Yule–Walker equations[38] for the autocorrelation function, $\rho_y(n) = \frac{E(y_s y_{s-n})}{v_y}$,

$$\rho_y(n) = \epsilon Z'(\psi) \sum_{k=1-n}^{C-n} \rho_y(k). \tag{23}$$

Using the basic properties of the autocorrelation function ($\rho_y(0) = 1$ and $\rho_y(n) = \rho_y(-n)$), the solution reads

$$\rho_y(n) = \frac{\epsilon Z'(\psi_C)}{1 - \epsilon Z'(\psi_C)(C-1)} \text{ for } 1 \le n \le C. \tag{24}$$

The capacities of the solutions involved in the dynamics scale with the feedback delay. Thus, for large delays, we have $\rho_y(n) \approx -\frac{1}{C}$, the inter-spike intervals within the delay line are weakly negatively correlated.

We obtain the variance of the distribution of ISIs v_y by multiplying Eq. (21) with itself and substituting the autocorrelation values. We find for the variance,

$$v_y = v_z \frac{1 - \epsilon Z'(\psi_C)(C-1)}{1 - \epsilon Z'(\psi_C)(C-1) - \epsilon^2 Z'(\psi_C)^2 C}, \tag{25}$$

which, for large capacities $C \gg \epsilon^{-1}$, reduces to $v_y \approx v_z/(1 + \epsilon Z'(\psi_C))$.

The Yule–Walker equations also allow us to compute the autocorrelation function for values $n > C$: for $n = C + 1$, we find

$$\begin{aligned} \rho_y(C+1) &= \epsilon Z'(\psi_C) \sum_{k=1}^{C} \rho_y(k) \\ &= \frac{C(\epsilon Z'(\psi_C))^2}{1 - \epsilon Z'(\psi_C)(C-1)} \\ &\approx -\epsilon Z'(\psi_C), \end{aligned} \tag{26}$$

meaning that the autocorrelation function $\rho_y(n)$ shows a peak around the delay time. This peak decays exponentially: for $n = C + m$, $(0 < m < C)$, we find

$$\begin{aligned} \rho_y(C+m) &= \epsilon Z'(\psi_C) \left(\sum_{k=m}^{C+m-2} \rho_y(k) + \rho_y(C+m-1) \right) \\ &\approx -\epsilon Z'(\psi_C) \left(1 + \epsilon Z'(\psi_C)\right)^{m-1}. \end{aligned} \tag{27}$$

We compare these theoretical predictions to numerical simulations of the stochastic system (9) in a wide range of parameters, for the sinusoidal PRC $Z(\theta) = \frac{1}{2\pi} \sin(2\pi\theta)$ and a delay $\tau = 100.5$ (which is large enough to use the simplified expressions for large delays). For this delay, the deterministic system always has a central solution with capacity $C^* = 100$, a reception phase $\psi_{100} = \frac{1}{2}$ and period $T_{100} = 1$, irrespective of the coupling strength ϵ. We used this solution as an initial condition and simulated until the oscillator reached 10^6 pulses.

In Fig. 5, we compare several statistics of the numerical data to the theoretical predictions. Figure 5(a) shows the autocorrelation function $\rho_y(n)$ of the ISIs, for the system fluctuating around the central state with $C^* = 100$. The agreement with the theoretical prediction is excellent: the autocorrelation function is very close to the small predicted value $-1/C^*$, except for the peaks at the multiples of $C^* + 1$. In Fig. 5(b), we show the variance of the inter-spike intervals for varying coupling strength ϵ and different noise intensities; again, the agreement with the theory is remarkable. Similarly, Fig. 5(c) shows the variance vs the noise intensity for fixed coupling strength $\epsilon = 0.5$. The theoretical approximation is very good for weak noise but deteriorates at $\sigma = \gamma \gtrsim 0.1$, which is to be expected as the theory relies on a weak noise approximation. A closer look at the system dynamics reveals that for such strong noise, the system starts hopping between different solutions. Although our theory does not apply in this case, in Sec. IV C, we show that it still allows us to calculate important characteristics of this hopping.

C. Hopping

The autoregressive model [Eqs. (21) and (22)] describes the dynamics when the system fluctuates around a single deterministic state, with a fixed capacity C. Nevertheless, it allows one to describe the switching events when the system escapes the basin of attraction of one deterministic state, and switches to another state. As indicated by the numerical simulations shown in Fig. 4, such a hopping event is indicated by the frequency ω_s passing an unstable state $\omega_u = \frac{\psi_u + C_s}{\tau}$, and, thus, it corresponds to the reception phase ψ_s reaching the unstable value ψ_u. Therefore, it is instructive to look at the deviations $w_s = \psi_s - \psi_C$ of the reception phase from its steady state value, given by Eq. (15),

$$w_s = x_s + \sigma \sqrt{\psi_C} \eta_1. \tag{28}$$

For weak noise, the reception phases are normally distributed around the deterministic value. Taking into account Eqs. (20) and (24), it is straightforward to obtain the variance v_w of the reception phases,

$$v_w = \gamma^2 + \sigma^2 \psi_C + v_y \frac{C}{1 - \epsilon Z'(\psi_C)(C-1)}. \tag{29}$$

For large delays, this simplifies to

$$v_w \approx \frac{T_C + \epsilon Z'(\psi_C)\psi_C}{-\epsilon Z'(\psi_C)(1 + \epsilon Z'(\psi_C))} \sigma^2 + \frac{1}{1 + \epsilon Z'(\psi_C)} \gamma^2. \tag{30}$$

A switching event corresponds to the reception phase ψ_s reaching an unstable state ψ_u, and this constitutes a large deviation from the deterministic value ψ_C. A linear approximation of the PRC is no longer valid; therefore, we avoid this restriction with a linear PRC,

$$Z(\theta) = \frac{1}{2} - \theta, \tag{31}$$

for which $Z'(\psi_C) = -1$ is constant, and, conveniently, $\psi_u = 0 = 1$, for all unstable solutions, irrespective of the capacity. This linear

Published under an exclusive license by AIP Publishing

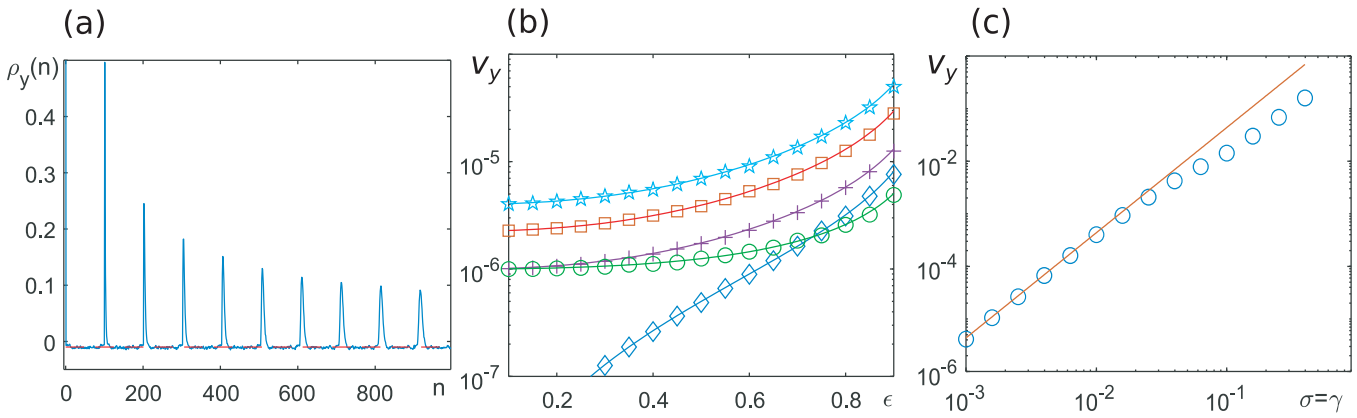

FIG. 5. Statistics of system (9)—numerical results vs the predictions of the weak noise theory, for system fluctuations around the state with $C^* = 100$. (a) The autocorrelation function $\rho_y(n)$. Red dashed line denotes the level $\rho_y = -1/100$. (b) The variance of the inter-spike intervals vs coupling strength ϵ for various values of the noise intensities: $\sigma = 0.001$ and $\gamma = 0$ (green circles), $\sigma = 0$ and $\gamma = 0.001$ (blue diamonds), $\sigma = \gamma = 0.001$ (magenta crosses), $\sigma = \gamma = 0.0015$ (red squares), and $\sigma = \gamma = 0.002$ (cyan asterisks.) Solid lines show the theoretical predictions. (c) The variance of the inter-spike intervals vs the noise intensity $\sigma = \gamma$ for fixed coupling strength $\epsilon = 0.5$. Blue circles: numerical results, red line: theoretical predictions. Other parameters are $\tau = 100.5$ and $Z(\theta) = \frac{1}{2\pi}\sin(2\pi\theta)$.

PRC is however unrealistic with respect to any real-world application.

For this PRC, a switching event corresponds to the reception phase exiting the interval $[0, 1]$: The capacity of the deterministic state increases by one when ψ_s exceeds one and decreases by one when ψ_s drops below zero. For long enough delays, the variance [Eq. (30)] is the same for all states,

$$\nu_w = \frac{\gamma^2}{1-\epsilon} + \sigma^2 \frac{2-\epsilon}{2\epsilon(1-\epsilon)}. \tag{32}$$

In order to obtain the switching statistics, one should solve the first passage time problem for autoregressive processes, which is highly nontrivial.[35] However, due to the low correlations for large delays, it is possible to estimate the switching rate as the probability to find a value of ψ_s beyond the boundary. Provided that ψ_s is normally distributed with mean ψ_C and variance ν_w, it is easy to estimate the probabilities $r_\pm(C)$ of switching to a solution with a higher or lower capacity,

$$r_+(C) \approx P(\psi_s > 1) = 1 - \Phi\left(\frac{1-\psi_C}{\sqrt{\nu_w}}\right), \tag{33}$$

$$r_-(C) \approx P(\psi_s < 0) = \Phi\left(\frac{-\psi_C}{\sqrt{\nu_w}}\right), \tag{34}$$

where $\Phi(x) = 0.5(1 + \mathrm{erf}(x/\sqrt{2}))$.

For weak noise, these probabilities are small, and using an approximation for the tails of the error function, we obtain

$$r_\pm(C) \approx \frac{\sqrt{\nu_w}}{2\sqrt{\pi}\Delta_\pm} \exp\left(-\frac{\Delta_\pm^2}{2\nu_w}\right), \tag{35}$$

where $\Delta_+ = 1 - \psi_C$ and $\Delta_- = \psi_C$ are the distances from ψ_C to 1 or 0, respectively.

In the following, we choose $\tau = C^* + 1/2$, where C^* is the capacity of the basic solution. For the linear PRC (31), this results in a period $T_{C^*} = 1$ and a reception phase $\psi_{C^*} = 1/2$ for this basic solution. The other solutions are arranged around the basic solution, the spectrum of solutions is similar to that of the sinusoidal PRC, mostly for the central solutions. Then, from Eq. (8), it is straightforward to show that for the linear PRC, the reception phases ψ_C of the different stable regimes are given by

$$\psi_C = \frac{1}{2} + \frac{C^* - C}{1 + \epsilon C}. \tag{36}$$

For the modes close to the central solution, and for large delays, we have $C - C^* \ll \tau$, so that we can approximate the distances $\Delta_\pm$ by

$$\Delta_\pm \approx \frac{1}{2} \pm \frac{C - C^*}{\epsilon\tau}, \tag{37}$$

and the switching rates $r_\pm(C)$ by

$$r_\pm(C) \approx \sqrt{\frac{\nu_w}{\pi}} \exp\left(-\frac{1}{8\nu_w}\right) \exp\left(\pm\frac{C^* - C}{2\nu_w\epsilon\tau}\right). \tag{38}$$

Here, we neglected the terms of the order τ^{-2} inside the exponent and the terms of the order τ^{-1} outside of the exponent. Then, the average lifetime of the stable mode with capacity C equals $L(C) = ((r_+(C) + r_-(C))^{-1}$ and can be approximated as

$$L(C) \approx \frac{1}{2}\sqrt{\frac{\pi}{\nu_w}} \exp\left(\frac{1}{8\nu_w}\right) \left[\cosh\left(\frac{C - C^*}{2\epsilon\nu_w\tau}\right)\right]^{-1}. \tag{39}$$

This result [Eq. (39)] for the average lifetime of different states reveals some major differences between the effect of both types of noise. For phase noise only, we have $\nu_w = \frac{2-\epsilon}{2\epsilon(1-\epsilon)}\sigma^2$ [see Eq. (30)]. This results in an approximate scaling of the lifetime of a central solution

$$L(C^*) \propto \exp\left(\frac{1}{8\sigma^2}\frac{2\epsilon(1-\epsilon)}{2-\epsilon}\right).$$

Published under an exclusive license by AIP Publishing

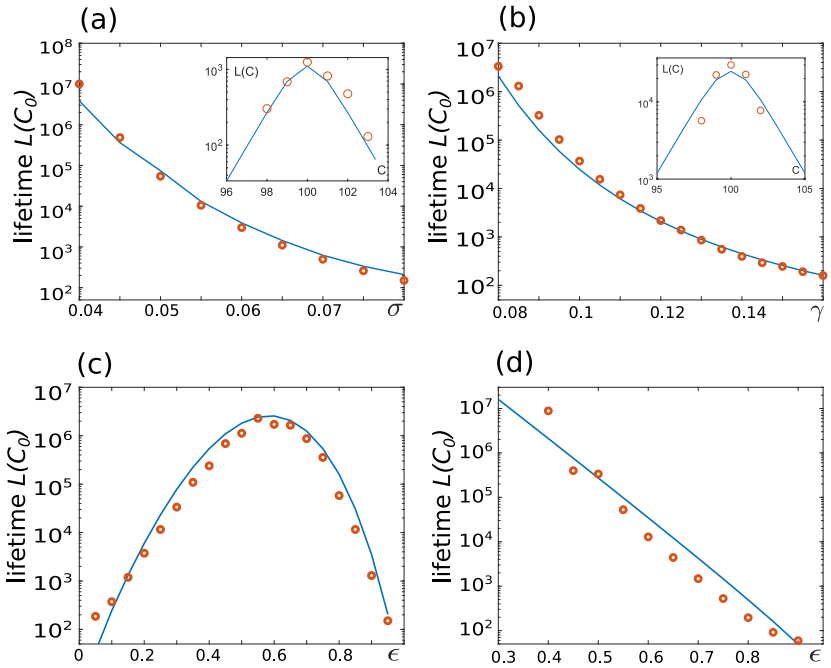

FIG. 6. Statistics of system (9) for hopping, for a linear PRC [Eq. (31)] and $\tau = 100.5$. (a) Average lifetime of the central solution $L(C^*)$ for varying phase noise strength σ, $\epsilon = 0.2$ and $\gamma = 0$. (b) $L(C^*)$ vs delay fluctuations γ, for $\epsilon = 0.4$ and $\sigma = 0$. (c) $L(C^*)$ vs the coupling strength ϵ, for $\sigma = 0.06$ and $\gamma = 0$. (d) $L(C^*)$ vs the coupling strength ϵ for $\gamma = 0.08$ and $\sigma = 0$. Blue lines—theoretical predictions (39) and red circles—numerical results. Insets in panels (a) and (b): lifetimes of different solutions vs their capacity for $\sigma = 0.06$ and $\gamma = 0.1$, respectively.

Thus, the lifetime $L(C^*)$ scales exponentially with σ^{-2}, and, for small coupling $\epsilon \ll 1$, we find that it increases exponentially with the coupling strength, $L(C^*) \propto e^{\frac{\epsilon}{8\sigma^2}}$.

If only the delay shows stochastic fluctuations, the linear theory predicts the opposite scaling: we have $\nu_w = \frac{\gamma^2}{1-\epsilon}$. This results in an exponential decrease of the lifetime with the coupling strength,

$$L(C^*) \propto \exp\left(\frac{1-\epsilon}{8\gamma^2}\right).$$

We compare the theoretical result for the lifetimes with numerical simulations of the oscillator with a linear PRC in Fig. 6. Here, we simulated the system until 10^4 switching events were detected. We show in Fig. 6(a) the lifetime of the central solution C^* vs the noise strength, for phase noise, while Fig. 6(b) shows the same results for stochastic delay fluctuations. The numerical results (red circles) fairly agree with the theoretical predictions (blue lines). The small discrepancy is not surprising, because of the many approximations applied. It should be noted that the discrepancy is higher for the side modes than for the central mode, as can be seen from the insets. The theory also predicts the scaling of the lifetime with coupling strength correctly, albeit with some discrepancies: Fig. 6(c) shows the lifetime of the central solution vs the coupling strength for phase noise, and Fig. 6(d) for stochastic delays: We find, as predicted by the theory, that the role of the coupling strength ϵ is strikingly different in the two scenarios. For the delay fluctuations, the lifetimes decrease exponentially with the coupling strength, while for the phase noise the dependence of the lifetimes on the coupling strength is non-monotonous. The system turns out to be most robust for intermediate coupling strength, while for small or large coupling the lifetimes vanish.

Theoretically, from the switching rates, one can also calculate the distribution over the different deterministic regimes, and from there, the width of frequency distribution. Assume detailed balance $p(C)r_+(C) = p(C+1)r_-(C+1)$ and note that $r_\pm(C) \sim \exp(\pm\beta(C^* - C))$, where $\beta = (2\nu_w\epsilon\tau)^{-1}$. Then, one can write

$$p(C^* + n) = p(C^*)\, e^{-\beta n^2}. \tag{40}$$

This defines a discrete normal distribution whose variance can be estimated as[36]

$$\nu_C \approx \epsilon\nu_w\tau. \tag{41}$$

Since $\omega_s = \frac{C_s+\psi_s}{\tau}$, we find for the variance of the frequency distribution,

$$\nu_\omega \approx \frac{\nu_C}{\tau^2} \approx \frac{\epsilon\nu_w}{\tau} \approx \left(1 + \frac{\epsilon}{2(1-\epsilon)}\right)\frac{\sigma^2}{\tau} + \frac{\epsilon}{1-\epsilon}\frac{\gamma^2}{\tau}. \tag{42}$$

Since the theoretical prediction of the lifetimes for side modes $C \neq C^*$ is not sufficiently accurate, Eq. (42) does not provide a good quantitative approximation for the width of the frequency distribution. However, the different dependency on both types of noise does explain some qualitative features we found in earlier work[29] for nonlinear PRCs.

V. SIMULATIONS

The theory developed above applies to a linear PRC, for which it does provide a good quantitative approximation for the lifetimes. Specifically, the linear model predicts a very different scaling of the hopping statistics with the coupling strength ϵ for both types of noise, as is shown in Fig. 6. In this section, we show that some of the main scaling properties that we found for the linear PRC

Published under an exclusive license by AIP Publishing

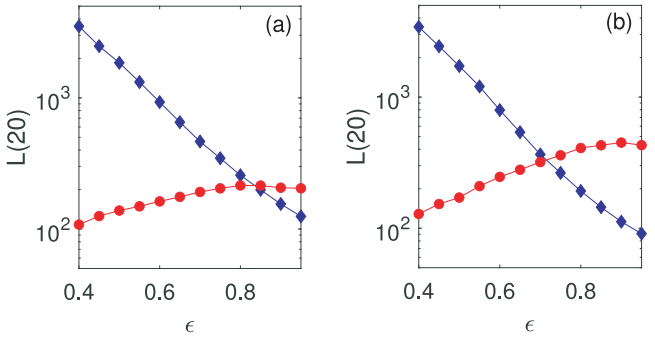

FIG. 7. Average lifetime of the central state with capacity $C = 20$; for phase noise (red circles), $\sigma = 0.1, \gamma = 0$ and for stochastic delays (blue diamonds), $\sigma = 0, \gamma = 0.17$; for the PRC, (a) $Z(\theta) = \frac{1}{2\pi}\sin(2\pi\theta)$, $\tau = 20.5$ and (b) $Z(\theta) = \frac{1}{2\pi}(1 - \cos(2\pi\theta))$, $\tau = 20.75 - 20\frac{\epsilon}{2\pi}$.

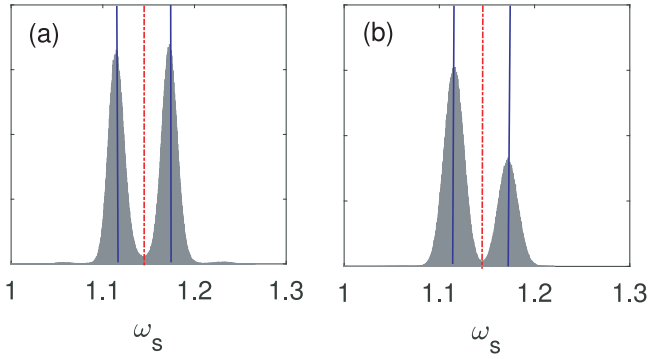

FIG. 9. Histogram of the frequency ω_s, for (a) phase noise $\sigma = 0.1$, $\gamma = 0$ and (b) stochastic delays, $\gamma = 0.11$, $\sigma = 0$. Other parameters are $\epsilon = 0.8$, $\tau = 15.95$, we used a PRC $Z(\theta) = \frac{1}{2\pi}(1 - \cos(2\pi\theta))$. The stable deterministic frequencies ω_{17} and ω_{18} are indicated by the full blue lines, and the red dotted-dashed line corresponds to the unstable state $\omega_u = \frac{\psi_u + 18}{\tau}$.

also apply to more realistic models. For this sake, we simulated the system [Eq. (9)] with the same two PRCs, the sinusoidal and the cosinusoidal ones. For stochastic delays, we averaged over up to $N = 50\,000$ hopping events; for phase noise, we recorded up to $N = 10\,000$ events.

For the sinusoidal PRC, we chose $\tau = 20.5$ and calculated the average lifetime of the central solution with capacity $C^* = 20$; note that we chose the delay such that for this state, irrespective of ϵ, we have $T_{20} = 1$, $\psi_{20} = \frac{1}{2}$. As $Z'(\psi_{20}) = -1$ does not change with the coupling strength, this choice allows us to study the role of ϵ without the need to adjust for a varying reception phase. The lifetime of this central state for varying ϵ is shown in Fig. 7(a): for phase noise only (red circles), we see an exponential increase of the lifetime with ϵ for small coupling, the lifetime then reaches a maximum and decreases slightly as $\epsilon \to 1$. This initial exponential increase is reminiscent of the stochastic switching properties for continuous coupling and additive noise,[30] which is not surprising since, for small

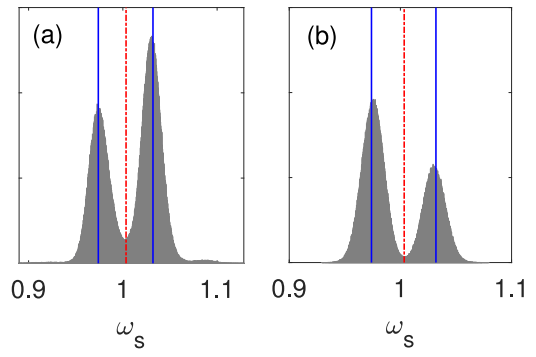

FIG. 8. Histogram of the frequency ω_s, for (a) phase noise, $\sigma = 0.1$, $\gamma = 0$ and (b) stochastic delays, $\gamma = 0.11$, $\sigma = 0$. Other parameters are $\epsilon = 0.8$, $\tau = 15.95$, we used a PRC $Z(\theta) = \frac{1}{2\pi}\sin(2\pi\theta)$. The stable deterministic frequencies ω_{15} and ω_{16} are indicated by the full blue lines, and the red dotted-dashed line corresponds to the unstable state $\omega_u = \frac{\psi_u + 16}{\tau}$.

ϵ, the pulse-coupled system can be approximated by a continuously coupled system.[11] It also corresponds to the behavior of the linear model. However, in contrast to the linear model, we only see a slight decrease of the lifetime as $\epsilon \to 1$. For stochastic delays (blue diamonds), we observe an exponential decrease of the lifetime with the coupling strength ϵ, similar to the linear model.

For the cosine PRC, we also compared the lifetime of the central state with capacity $C = 20$, and in this case, $\psi_{20} = \frac{3}{4}$. In order to keep ψ_{20} constant as the coupling increases, we adjust the delay to $\tau = 20.75 - 20\frac{\epsilon}{2\pi}$. The lifetimes only depend weakly on the delay, and this dependency disappears as the delay increases; we have shown this numerically in earlier work,[29] and this property appears in the linear theory [Eq. (29)] as well as for continuous coupling.[30] We find qualitatively similar scaling of the lifetimes for both PRCs: also for the cosine PRC, shown in Fig. 7(b), we see an exponential decrease of the lifetimes with increasing ϵ for stochastic delays, and an initial exponential increase, followed by a slight decrease, for phase noise.

In the linear model, we use a constant and negative $Z'(\cdot)$; this assumption certainly does not apply to the sinusoidal PRC or to the cosine PRC around the switching points ψ_u, and the linear model can, therefore, only be expected to provide qualitative information. However, the linear model does explain the qualitative difference between the scaling properties of both types of noise. Indeed, while for phase noise the lifetimes is non-monotonically dependent on the coupling strength with a maximum at the intermediate values, they monotonically decrease with the coupling strength for stochastic delays.

The two different types of noise do not only result in different switching statistics. In Fig. 8, we compare the distributions of ω_s for a sinusoidal PRC due to phase noise and stochastic delays. All other parameters, and, hence, the deterministic solutions are the same, and, in both cases, the system switches between the solutions with $C = 15$ and with $C = 16$. Note, however, that in the frequency distribution due to phase noise [shown in panel (a)], the faster state with $C = 16$ is attended most often, while for stochastic delays [shown

Published under an exclusive license by AIP Publishing

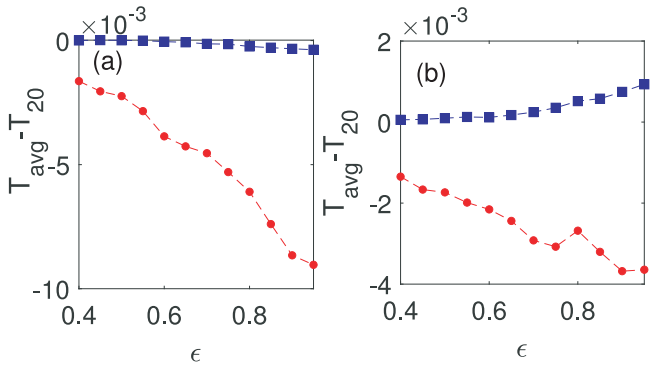

FIG. 10. Deviation of the average ISI $T_{avg} - T_{20}$, over 10^7 spikes or 50 000 switching events (whichever occurs sooner) for phase noise $\sigma = 0.1$, $\gamma = 0$ (red squares) and stochastic delays, $\gamma = 0.17$, $\sigma = 0$ (blue circles). Other parameters are for panel (a) $\tau = 20.5$, we used a PRC $Z(\theta) = \frac{1}{2\pi}\sin(2\pi\theta)$ and panel (b) $\tau = 20.75 - \frac{\epsilon}{2\pi}$ and $Z(\theta) = \frac{1}{2\pi}(1 - \cos(2\pi\theta))$.

in panel (b)], the peak at the slower solution $C = 15$ is highest. For larger delays and a more symmetric set of solutions, we also see an effect in the lifetimes. The faster solutions have a longer lifetime than their slower counterparts for the same $Z'(\psi_C)$ (not shown).

This shift of the frequency distribution toward faster solutions is also present for the cosine PRC, as is shown in Fig. 9. In this case, the system has a slower solution with $C = 17$ and a faster one with $C = 18$. While for phase noise [panel (a)] both states are almost equally often attended, the system has a preference for the slower regime for stochastic delays [panel (b)].

We quantify this effect in Fig. 10: we compare the average ISI over the whole time trace to the ISI of the central solution with $C = 20$, for the same parameters as Fig. 7. For the sinusoidal PRC, shown in Fig. 10(a), when there is only a stochastic delay, the average ISI stays very close to the ISI of the central state $T_{20} = 1$ for all values of the coupling. This means that the distribution of the

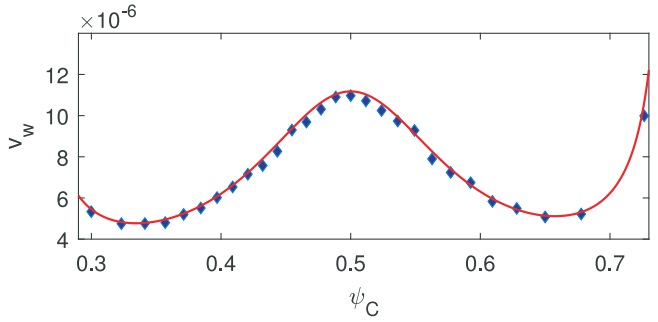

FIG. 11. Variance v_w of the reception phase around the different deterministic states (blue diamonds), for 2×10^5 pulses each. The deterministic states have capacities $C = 85 - 112$. The red curve is the weak noise approximation [Eq. (30)]. The parameters are chosen such that no switching occurs, $\tau = 100.5$, $\epsilon = 0.85$, $\gamma = \sigma = 10^{-3}$, and the PRC is given by $Z(\theta) = \frac{1}{2\pi}\sin(2\pi\theta)$.

frequencies is symmetric around this central frequency $\omega = 1$. In contrast, for phase noise, the average ISI decreases as the coupling increases, showing that the system shifts toward higher frequencies.

In Fig. 10(b), we show similar results for the cosine PRC. The set of solutions is not symmetrical in this case (see Fig. 2) and both for phase noise and stochastic delay, the average ISI deviates from the central solution T_{20} as the coupling increases. However, we see again that in the presence of phase noise, the average ISI is clearly smaller than due to stochastic delays, and this difference grows with the coupling strength.

This peculiar effect of speeding up by phase noise can to some extent be deduced from the expression for the variance [Eq. (30)] of the reception phases in the weak noise approximation: the contribution to the variance due the stochastic delays, which is proportional to γ, only depends on $Z'(\psi_C)$. For the sinusoidal PRC, this results in a variance being symmetric around $\psi_C = \frac{1}{2}$.

When including the phase noise term, proportional to σ^2, the dependency on ψ_C is more complicated. We show the variance v_w of the reception phases ψ_s in Fig. 11, for sinusoidal coupling, and equal contributions of both types of noise, the numerical data for a large delay (blue diamonds) and the theoretical value (full red line) correspond very well. The dependency is non-monotonous, and in particular, it is asymmetric: the faster regimes, with a shorter ISI T_C and a reception phase $\psi_C \in \left(\frac{1}{4}, \frac{1}{2}\right)$, typically have a smaller variance than the slower regimes [for the same $Z'(\psi_C)$]—the size of this effect depends on the coupling strength and the precise shape of the PRC.

VI. CONCLUSION

In this paper, we present a detailed study of a phase oscillator with pulse delayed feedback subject to two types of noise: additive phase noise acting on the oscillator and stochastic fluctuations of the coupling delay. Pulse-coupled oscillators are a well-known example of non-smooth dynamics since their state undergoes abrupt jumps when they receive pulses. The presence of such jumps allows us to develop event-based techniques, which describe the system evolution from one pulse to another. Here, we extend this event-based approach to noisy systems and suggest an integration scheme based on a stochastic map. This scheme allows efficient and fast simulation of the system in the presence of either or both noise sources.

We mostly concentrate on the case of large enough delays, when there is a range of coupling strengths, for which the system has multiple coexisting stable regimes. These regimes are characterized by a constant interspike interval, constant temporal capacity, constant reception phase, and constant frequency. We show that in the limit of weak noise, the system fluctuates around one of the deterministic states; in that case, the dynamics can be described as an autoregressive process. This allows us to analytically calculate the magnitude of the fluctuations and the autocorrelation function. We show that these analytical results are in good agreement with numerical simulations. For large delays, the autocorrelation function of the ISI time series resembles the typical pattern of chaotic systems with a large feedback delay, with reappearing peaks at multiples of the delay time.[37]

As the noise strength increases, the system starts to deviate significantly from the deterministic solutions, which naturally leads to

Published under an exclusive license by AIP Publishing

a collapse of the linear theory. The most interesting effects are then observed in the presence of multistability: the noisy system starts to switch sporadically between different deterministic solutions. Surprisingly, the linear theory still provides relevant information on this switching: In the particular case of a linear PRC, it allows one to estimate the lifetimes of different solutions and their scaling with system parameters, such as noise strength and coupling strength.

Our theory reveals a number of nontrivial effects, which underline the key difference between the two types of noise. Surprisingly, the scaling of the lifetimes with the coupling strength turns out to be the opposite for phase noise and for stochastic delays. In particular, the lifetimes decrease exponentially with the coupling strength for stochastic delays, while for phase noise, they initially increase exponentially and reach a maximum for intermediate coupling strength, after which they steeply decrease.

These scaling properties predicted by the linear theory also hold for general, nonlinear PRCs. We simulated an oscillator with a sinusoidal PRC, and one with a cosine-shaped PRC, and found the same qualitative scaling as for the linear PRC: The lifetimes decrease exponentially with the coupling strength for stochastic delays, and for additive phase noise they initially increase exponentially, similar to the continuously coupled system, but, in contrast to continuously coupled systems, they reach a maximum for intermediate coupling. In contrast to the linear PRC, the lifetimes do not vanish as $\epsilon \to 1$. We attribute this discrepancy to the fact that the system with nonlinear PRC shows a multijitter bifurcation.[27]

The numerical simulations also reveal another characteristic effect of phase noise: it speeds up the dynamics, i.e., phase noise makes the system prefer solutions with higher frequencies. For stochastically varying delays, this effect is much smaller or even opposite.

To conclude, the achievement of this paper is twofold. First, we propose an event-based integration scheme applicable to pulse-coupled systems in the presence of different types of noise. While the analytical treatment and numerical methods for additive phase noise are well established, the influence of stochastic delays has not yet been extensively explored. Our event-based approach allows a straightforward implementation of both noise sources and allows us to establish an analytical framework to estimate the switching statistics. Second, we demonstrate that the effects of phase noise and delay fluctuations can be drastically different: we show this analytically with a linear PRC, and our theory shows good correspondence to numerical simulations. We show numerically qualitatively similar scaling results for two different nonlinear PRCs.

Our results can potentially be applied to more complex systems, such as networks of pulse-coupled oscillators to which the event-based approach can be easily generalized. Based on our results, we expect/hypothesize that in such networks, the action of the noise on the nodes (oscillators) and the links (delay lines) might lead to different effects, and this is worth further study.

ACKNOWLEDGMENTS

The work of V.V.K. was funded by the RSF (Grant No. 19-12-00338).

AUTHOR DECLARATIONS

Conflict of Interest

The authors have no conflicts to disclose.

Author Contributions

Vladimir V. Klinshov: Conceptualization (equal); Data curation (equal); Formal analysis (equal); Funding acquisition (equal); Investigation (equal); Methodology (equal); Project administration (equal); Resources (equal); Software (equal); Supervision (equal); Validation (equal); Visualization (equal); Writing – original draft (equal); Writing – review & editing (equal). **Otti D'Huys:** Conceptualization (equal); Data curation (equal); Formal analysis (equal); Funding acquisition (equal); Investigation (equal); Methodology (equal); Project administration (equal); Resources (equal); Software (equal); Supervision (equal); Validation (equal); Visualization (equal); Writing – original draft (equal); Writing – review & editing (equal).

DATA AVAILABILITY

The data that support the findings of this study are available from the corresponding author upon reasonable request.

REFERENCES

[1] P. Dayan and L. F. Abbott, *Theoretical Neuroscience* (MIT Press, Cambridge, MA, 2001).
[2] C.-H. Luo and Y. Rudy, Circ. Res. **68**, 1501 (1991).
[3] R. Pagliari, Y. P. Hong, and A. Scaglione, IEEE J. Sel. Areas Commun. **28**, 564 (2010).
[4] A. Lopera, J. M. Buldú, M. C. Torrent, D. R. Chialvo, and J. García-Ojalvo, Phys. Rev. E **73**, 21101 (2006).
[5] D. P. Rosin, D. Rontani, D. J. Gauthier, and E. Schöll, Phys. Rev. Lett. **110**, 104102 (2013).
[6] O. D'Huys, J. Lohmann, N. D. Haynes, and D. J. Gauthier, Chaos **26**(9), 094810 (2016).
[7] D. A. Safonov, V. V. Klinshov, and V. K. Vanag, Phys. Chem. Chem. Phys. **19**, 12490 (2017).
[8] P. Colet and R. Roy, Opt. Lett. **19**, 2056 (1994).
[9] C. C. Canavier and S. Achuthan, Math. Biosci. **226**, 77 (2010).
[10] R. E. Mirollo and S. H. Strogatz, SIAM J. Appl. Math. **50**, 1645 (1990).
[11] P. Goel and B. Ermentrout, Physica D **163**, 191 (2002).
[12] L. F. Abbott and C. Van Vreeswijk, Phys. Rev. E **48**, 1483 (1993).
[13] W. Gerstner, Neural Comput. **12**, 43 (2000).
[14] S. Achuthan and C. C. Canavier, J. Neurosci. **29**, 5218 (2009).
[15] L. Lücken and S. Yanchuk, Physica D **241**, 350 (2012).
[16] R. Zillmer, R. Livi, A. Politi, and A. Torcini, Phys. Rev. E **76**, 46102 (2007).
[17] V. V. Klinshov and V. I. Nekorkin, Commun. Nonlinear Sci. Numer. Simul. **18**, 973 (2013).
[18] V. Klinshov and V. Nekorkin, Chaos **27**, 101105 (2017).
[19] U. Ernst, K. Pawelzik, and T. Geisel, Phys. Rev. Lett. **74**, 1570 (1995).
[20] U. Ernst, K. Pawelzik, and T. Geisel, Phys. Rev. E **57**, 2150 (1998).
[21] M. M. Woodman and C. C. Canavier, J. Comput. Neurosci. **31**, 401 (2011).
[22] V. V. Klinshov and V. I. Nekorkin, Chaos Soliton. Fract. **44**, 98 (2011).
[23] C. C. Canavier and R. A. Tikidji-Hamburyan, Phys. Rev. E **95**, 032215 (2017).
[24] V. Klinshov, L. Lücken, and S. Yanchuk, Eur. Phys. J. Spec. Top. **227**, 1117 (2018).
[25] J. Foss, A. Longtin, B. Mensour, and J. Milton, Phys. Rev. Lett. **76**, 708 (1996).
[26] J. Foss and J. Milton, J. Neurophysiol. **84**, 975 (2000).

Published under an exclusive license by AIP Publishing

[27]V. Klinshov, L. Lücken, D. Shchapin, V. Nekorkin, and S. Yanchuk, Phys. Rev. Lett. **114**, 178103 (2015).
[28]V. Klinshov, L. Lücken, D. Shchapin, V. Nekorkin, and S. Yanchuk, Phys. Rev. E **92**, 042914 (2015).
[29]V. Klinshov, D. Shchapin, and O. D'Huys, Phys. Rev. Lett. **125**, 034101 (2020).
[30]O. D'Huys, T. Jüngling, and W. Kinzel, Phys. Rev. E **90**, 032918 (2014).
[31]E. Brown, J. Moehlis, and P. Holmes, Neural Comput. **16**, 673 (2004).
[32]G. B. Ermentrout and N. Kopell, SIAM J. Appl. Math. **46**, 233–253 (1986).
[33]C. Masoller, Phys. Rev. A **50**, 2569 (1994).
[34]D. R. Cox and H. D. Miller, *The Theory of Stochastic Processes* (Routledge, New York, 1965).
[35]E. Di Nardo, Sci. Math. Jpn. Online **e-2008**, 61–76 (2008).
[36]P. Szabłowski, Stat. Probab. Lett. **52**, 289 (2001).
[37]X. Porte, O. D'Huys, T. Jüngling, D. Brunner, M. C. Soriano, and I. Fischer, Phys. Rev. E **90**, 052911 (2014).
[38]C. Chatfield, *The Analysis of Time Series: An Introduction*, 6th ed. (Chapman and Hall, 2003).

Published under an exclusive license by AIP Publishing